JACS
JOURNAL OF THE AMERICAN CHEMICAL SOCIETY
Article
pubs.acs.org/JACS

Atomistic Theory of Ostwald Ripening and Disintegration of Supported Metal Particles under Reaction Conditions

Runhai Ouyang, Jin-Xun Liu, and Wei-Xue Li*

State Key Laboratory of Catalysis, Dalian Institute of Chemical Physics, Chinese Academy of Sciences, Dalian 116023, China

Supporting Information

ABSTRACT: Understanding Ostwald ripening and disintegration of supported metal particles under operating conditions has been of central importance in the study of sintering and dispersion of heterogeneous catalysts for long-term industrial implementation. To achieve a quantitative description of these complicated processes, an atomistic and generic theory taking into account the reaction environment, particle size and morphology, and metal−support interaction is developed. It includes (1) energetics of supported metal particles, (2) formation of monomers (both the metal adatoms and metal−reactant complexes) on supports, and (3) corresponding sintering rate equations and total activation energies, in the presence of reactants at arbitrary temperature and pressure. The thermodynamic criteria for the reactant assisted Ostwald ripening and induced disintegration are formulated, and the influence of reactants on sintering kinetics and redispersion are mapped out. Most energetics and kinetics barriers in the theory can be obtained conveniently by first-principles theory calculations. This allows for the rapid exploration of sintering and disintegration of supported metal particles in huge phase space of structures and compositions under various reaction environments. General strategies of suppressing the sintering of the supported metal particles and facilitating the redispersions of the low surface area catalysts are proposed. The theory is applied to TiO_2(110) supported Rh particles in the presence of carbon monoxide, and reproduces well the broad temperature, pressure, and particle size range over which the sintering and redispersion occurred in such experiments. The result also highlights the importance of the metal−carbonyl complexes as monomers for Ostwald ripening and disintegration of supported metal catalysts in the presence of CO.

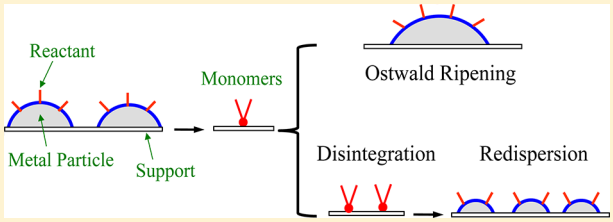

1. INTRODUCTION

Transition metals have been used to catalyze a wide range of chemical reactions in heterogeneous catalysis, which plays an important role in energy conversion, chemicals production, and environmental protection. To be more accessible to reactants, transition metal catalysts are usually dispersed on a high surface area support, and corresponding size falls typically in the range of nanometers.[1] Although dispersed metal particles expose a large number of low coordination sites which could act as the active sites and greatly enhance the catalytic activity,[2−6] a high ratio of these low coordination sites destabilizes the dispersed metal particles in the meantime. Thus, the metal particles tend to agglomerate and/or sinter, either by coalescence of smaller particles or by Ostwald ripening for the growth of a larger particle at the expense of a smaller one.[7−11] In the end, the overall activity of the metal particles decreases with time and eventually deactivates due to the loss of the active surface area. To prevent the sintering, the proper supports should be selected to stabilize the metal particles by means of the metal−support interaction (MSI), but so far, its utilization is achieved mainly by trial and error.[12,13] To increase the lifetime of industrial catalysts, it is important to know how to suppress the particle sintering rate and how to redisperse the deactivated catalysts due to the sintering. A fundamental understanding of the sintering mechanism and kinetics at the microscopic level would be highly valuable to provide insight into controlling these processes.

The study of sintering is further complicated by considering catalytic reactions usually operated at elevated temperatures and pressures.[14−17] The presence of reactants could affect and/or induce dramatically the sintering, disruption, and dispersion of supported metal particles,[18−27] as well as the crystalline surfaces.[28−34] For instance, it was found that, under elevated carbon monoxide (CO) partial pressures, supported Rh particles were readily disintegrated to the mononuclear Rh-carbonyl complexes.[35−40] At higher temperature, the Rh complexes decomposed, and the Rh adatoms released started to agglomerate and form larger metal particles. Similarly, reactant-assisted ripening and disintegration had also been found when supported metal particles were exposed to oxygen,[41−47] and the reason was attributed to the formation of volatile oxygen−metal complexes. It has also been suggested that reactants could change the wetting behavior of metal particles, causing them to spread out on supports when the adsorbate−metal bond energy exceeds the difference in energy between the metal−metal and metal−support bonding.[48,49] Moreover, the strong interaction between adsorbate and metal

Received: September 2, 2012
Published: December 31, 2012

dx.doi.org/10.1021/ja3087054 | J. Am. Chem. Soc. 2013, 135, 1760−1771

particle could weaken the metal−metal bond,[50] which would facilitate the detachment of the metal adatoms from small particles, and eventually promote sintering and disintegration.

Despite extensive studies so far, a clear mechanistic understanding and a quantitative description of reactants on the sintering and disintegration of supported metal particles remains missing. Sintering kinetics of supported metal particles and the elementary steps involved was pioneered by Wynblatt and Gjostein (WG).[7,8] Although sintering in the presence of an oxygen environment and the formation of the oxygen−metal complexes as the transient monomers was studied in this work, it is unclear yet when the metal−reactant complexes rather than the metal adatoms as dominant monomers will form under the reaction conditions. In particular, how will the formation of the metal−reactant complexes depend on the reaction conditions, the metal particle size and shape, and the MSI? How will the metal−reactant complexe formation affect the ripening kinetics and the underlying mechanism? The formation of the metal−reactant complexes may also be involved deeply in the reactant induced disintegration, a fact that has been used widely to redisperse the low surface area metal catalysts due to the sintering.[27,51−55] It is therefore important to disentangle the role of the metal−reactant complexes in the reactant assisted ripening and induced disintegration of supported metal particles.

Here, we will focus on Ostwald ripening using a surface diffusion model, for which the elementary steps typically include detachment of the metal atoms from smaller particles to form monomers, diffusion of monomers on supports, and attachment toward larger particles. A major improvement of the WG theory following the Ostwald ripening model was obtained by Campbell and co-workers by incorporating size-dependent surface energy in their model and using an exponential function in the formulation of the ripening rate instead of a first-order approximation of the associated Talyor series.[11,56] It was found that surface energy and morphology of supported metal particles are sensitive to the reaction environments,[57−59] a fact that could affect the ripening process.[60] However, a theory of sintering and disintegration accounting for the influence of reactant adsorption on surface energy and morphology of the supported metal particles is not available yet.

To address these questions, an atomistic theory of Ostwald ripening and disintegration of supported metal particles in the presence of reactants was developed and is first presented in section 2. We propose that the strong bonding between the reactant and metal adatom on supports is essential for the formation of metal−reactant complexes. Surface energy and chemical potential of supported metal particles with adsorption of reactants are derived, and the thermodynamic variables describing the adsorption of reactants on adatoms and formation of the metal−reactant complexes on support are defined. The criteria for reactant assisted Ostwald ripening and induced disintegration are formulated, and corresponding rate equations are derived. The theory is applied to $TiO_2(110)$ supported Rh particles under CO in Section 3, and most parameters required are calculated by first-principles theory. Influence of CO on sintering and disintegration of supported Rh particles is studied under a wide range of particle sizes and reaction conditions. A brief summary is given in Section 4.

2. THEORETICAL FORMALISM

2.1. Energetics of Supported Particles. Under operating conditions, reactants may adsorb on supported metal particles and affect their morphology and stability, which is closely related to subsequent Ostwald ripening and disintegration. It is therefore important to quantify the energetics of the supported metal particles in the presence of reactants.

To study this, we start from the energetics of a supported metal particle in the absence of reactants. As shown schematically in Figure 1, a supported metal particle in a spherical segment can be described by the radius of curvature R, contact angle α with respect to the support, exposed surface area of the spherical segment $A_s = 2\pi R^2[1 - \cos(\alpha)]$, and contact interface area between particle and support $A_{int} = \pi R^2 \sin^2(\alpha)$. Average energy ΔE_{NP} (per atom) with respect to infinite size particle (bulk) can be calculated by

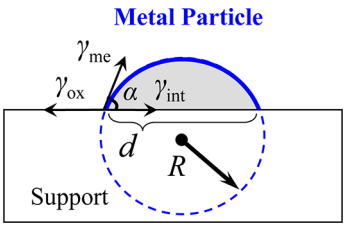

Figure 1. Schematic of supported metal particle in a spheric segment with the radius of curvature R and the contact angle α between the particle and support. γ_{me}, γ_{ox}, and γ_{int} are the surface energies of the metal particle and support, and the interface energy between metal particle and support, respectively. d is the projected diameter of the metal particle on support.

$$\Delta E_{NP} = \frac{1}{N}[(A_s + A_{int})\gamma_{me} + A_{int}H_{adh}] \quad (1)$$

where $N = 4\pi R^3\alpha_1/3\Omega$ is the number of the metal atoms in the particle of interest, and Ω is the molar volume of bulk metal atom, and $\alpha_1 = [2 - 3\cos(\alpha) + \cos^3(\alpha)]/4$. γ_{me} is surface energy of the metal particle, $H_{adh} = \gamma_{int} - \gamma_{me} - \gamma_{ox}$ is adhesion energy between the metal particle and support, γ_{int} is interfacial energy between the metal particle and support, and γ_{ox} is surface energy of the support. Based on the Young equation, $\cos(\alpha)\gamma_{me} = \gamma_{ox} - \gamma_{int}$, one has $H_{adh} = -[1 + \cos(\alpha)]\gamma_{me}$. Accordingly, ΔE_{NP} can be reformulated as

$$\Delta E_{NP} = \frac{1}{N}[A_s - A_{int}\cos(\alpha)]\gamma_{me} = \frac{3\Omega\gamma_{me}}{R} \quad (2)$$

Considering that metal particles may expose different facets i with surface energy γ_i and corresponding area ratio f_i over the whole surface area, the overall surface energy γ_{me} could be rewritten as

$$\gamma_{me} = \sum_i f_i \times \gamma_i \quad (3)$$

The chemical potential (differentiate energy) $\Delta\mu_{NP}$ of the supported metal particle can be derived

$$\Delta\mu_{NP} = \frac{d}{dN}(N \times \Delta E_{NP}) = \frac{2\Omega\gamma_{me}}{R} \quad (4)$$

This equation is often noted as the Gibbs−Thomson (G−T) relation in the literature.[7,11,42,61]

Both the average energy and the chemical potential of the particle defined by eq 2 and eq 4 are proportional to the reciprocal of the radius of curvature R and the surface energy γ_{me}. Namely, a particle with a smaller radius of curvature R and higher surface energy would have higher energies and chemical

dx.doi.org/10.1021/ja3087054 | J. Am. Chem. Soc. 2013, 135, 1760−1771

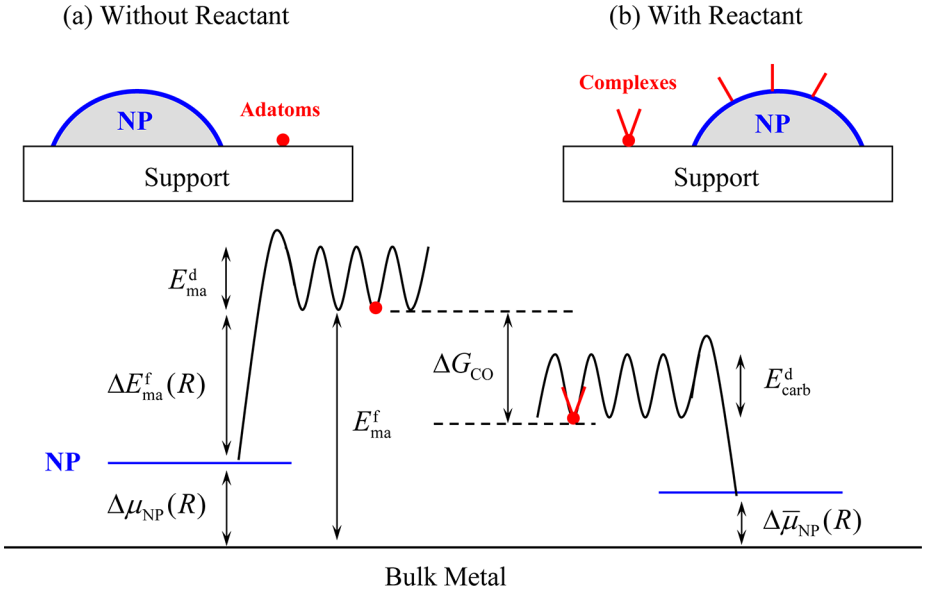

Figure 2. Energetic diagram of supported metal particles without (a) and with (b) the presence of reactants. Here, $\Delta\mu_{NP}(R)$ and $\Delta\bar{\mu}_{NP}(R)$ are the chemical potentials of supported metal particles, E^{f}_{ma} and $\Delta E^{f}_{ma}(R)$ are the formation energies of monomers (the metal adatoms) on support with respect to infinite and finite size metal particle, ΔG_{CO} is the Gibbs free energy of adsorption of reactants (CO in present work) on the metal adatom, and E^{d}_{ma} and E^{d}_{carb} are the diffusion barriers of monomers (the metal adatoms and the metal−reactant complexes) on support.

potential. Dependence of $1/R$ comes from the fact that the extent of destabilization is proportional to the ratio of surface atoms over the total number of the atoms in the particle.[4,62,63] We note that the MSI, which is essential to the stability of the dispersed metal particles, is included implicitly in these equations. To see this clearly, we consider a mass (volume) conserved particle containing N metal atoms deposited on a certain support. Since a different support might have a rather different MSI, the contact angle α (and α_1) could change. Based on $N = 4\pi R^3\alpha_1/3\Omega$, the radius of curvature R would change, and so on for the corresponding ΔE_{NP} and $\Delta\mu_{NP}$. Stronger MSI (larger adhesion energy H_{adh}) would lead to smaller α (and α_1) and larger R, and eventually lower ΔE_{NP} and $\Delta\mu_{NP}$. When $\alpha \to 0$, $R \to \infty$ and thus both ΔE_{NP} and $\Delta\mu_{NP}$ approach zero. In this limit, the metal particles would wet the support forming a two-dimensional film, and not experience the Gibbs−Thomson effect anymore. Corresponding energetics are bulk-like, or even lower when the interaction between the metal and support is stronger than that of the metal−metal bond.[49]

Under reaction conditions, reactants may adsorb on the metal particles, and corresponding Gibbs free energy of the adsorption would reduce the surface energy and stabilize the metal particles. Using CO as an example, the reduction of surface energy $\Delta\gamma_i$ on the facet i at given temperature T and partial pressure P can be calculated[28]

$$\Delta\gamma_i(T, P) = \theta_i[E^{ad}_{CO}(\theta_i) - \Delta\mu_{CO}(T, P)]/A_i \quad (5)$$

where θ_i and A_i is the coverage of adsorbed CO and surface unit area of the facet i. $E^{ad}_{CO}(\theta_i)$ is the average binding energy of CO and coverage dependent. The chemical potential of CO in gas phase is $\Delta\mu_{CO}(T, P) = \Delta\mu^{\circ}_{CO}(T, P^{\circ}) + kT\ln(P/P^{\circ})$, where k is the Boltzmann constant, and $\Delta\mu^{\circ}_{CO}(T,P^{\circ})$ is the chemical potential of CO at standard condition P°.[64,65] For reactants at a given T and P, the corresponding coverage θ_i can be determined by

$$E^{dif}_{CO}(\theta_i) = \frac{d[\theta_i \times E^{ad}_{CO}]}{d\theta_i} = \Delta\mu_{CO}(T, P) \quad (6)$$

where $E^{dif}_{CO}(\theta_i)$ is the differential binding energy of reactants. Dependence of E^{ad}_{CO} and E^{dif}_{CO} on θ_i can be obtained from the experiment or first-principles theory calculation.

The effective surface energy $\bar{\gamma}_{me}$ of supported metal particles with adsorbates (the symbol with bar represents the variables in the presence of reactants and adopted below without mention otherwise) becomes

$$\bar{\gamma}_{me}(T, P) = \sum_i f_i[\gamma_i + \Delta\gamma_i(T, P)] \quad (7)$$

By substituting $\bar{\gamma}_{me}$ in eq 2 and eq 4, average energetics $\Delta\bar{E}_{NP}$ and chemical potential $\Delta\bar{\mu}_{NP}$ of supported metal particles under reactants can be obtained, respectively.

Equations 3 and 7 could be used to construct the equilibrium morphology of the metal particle in the absence and presence of reactants. By minimizing the overall surface energies, the exposed facet i and ratio f_i could be determined. It is clear that, in the presence of reactants, the morphology of the metal particle could change, as documented in the literature.[57−59] It is important to note that the particle surface energy and chemical potential now becomes a function of T and P. This will affect the sintering of the supported metal particles[60] and is included in following derivation.

2.2. Ostwald Ripening. As indicated earlier, we focus in the present work on sintering dominated by surface Ostwald ripening, whereby the metal atoms detach from small particles with high chemical potential as monomers, diffuse on the support, and subsequently attach to larger particles with a lower chemical potential. This leads to the growth of larger particles at the expense of smaller particles. The latest derivation of the kinetic equation of Ostwald ripening in the absence of reactants can be found in the work of Campbell and co-workers.[11] For completeness and consistency with the following derivation in

dx.doi.org/10.1021/ja3087054 | J. Am. Chem. Soc. 2013, 135, 1760−1771

the presence of reactants, we introduce here the key points with a slightly different convention.

We start from the formation energy of the metal adatoms as monomers on the support. Corresponding energetics not only affect the barrier of the detachment/attachment of the metal atoms from/toward the metal particles as discussed below, but also determine the concentration of monomers formed, which both are crucial for the sintering rate. The formation energy ΔE^{f}_{ma} of the metal adatoms with respect to a metal particle of radius R (see Figure 2a) is

$$\Delta E^{f}_{ma}(R) = E^{f}_{ma} - \Delta\mu_{NP}(R) \tag{8}$$

$$E^{f}_{ma} = E_{ma/ox} - E_{ox} - E_{B} \tag{9}$$

where E^{f}_{ma} is the formation energy of the metal adatoms with respect to infinite size metal (bulk like) particle, $E_{ma/ox}$ is the total energy of the metal adatom on support, E_{ox} is the total energy of the support, and E_B is the total energy of the bulk metal. Alternatively, E^{f}_{ma} can be calculated from the cost of the sublimation enthalpy of bulk metal plus subsequent energy gain from the adsorption of an isolated metal atom on the support.[11]

The concentration, $c_s(R)$, of the metal adatoms in equilibrium with a finite size metal particle of radius R in the far-field limit (neglecting the contribution of small vibrational enthalpy[65]) is therefore written

$$c_s(R) = \frac{1}{a_0^2}\exp\left[\frac{-\Delta E^{f}_{ma}(R)}{kT}\right] = c_s^{eq}\exp\left[\frac{\Delta\mu_{NP}(R)}{kT}\right] \tag{10}$$

where $c_s^{eq} = \exp[-E^{f}_{ma}/kT]/a_0^2$ is the concentration of the metal adatoms in equilibrium with respect to the infinite size metal particle in the far-field limit, a_0 is the lateral lattice constant of support.

Under the steady state for which the time rate of concentration of the metal adatoms immediately adjacent to a particle is equal to zero, the time rate equation dR/dt of the metal particles of radius R could be derived

$$\frac{dR}{dt} = \frac{XY}{X+Y}\frac{K}{R^2}\exp\left[\frac{-E_{tot}}{kT}\right]\left(\exp\left[\frac{\Delta\mu_{NP}(R^*)}{kT}\right] - \exp\left[\frac{\Delta\mu_{NP}(R)}{kT}\right]\right) \tag{11}$$

and E_{tot} is the total activation energy,

$$E_{tot} = E^{d}_{ma} + E^{f}_{ma} \tag{12}$$

where E^{d}_{ma} is the diffusion barrier of monomers on support, $K = \nu_s\Omega/[4\pi a_0^2\alpha_1]$, $X = 2\pi a_0 R\sin(\alpha)$, $Y = 2\pi a_0^2/\ln[L/(R\sin(\alpha))]$, ν_s is vibrational frequency of the monomer on support, L is diffusion length required for the monomer concentration on support to reach its far field limit of $c_s(R^*)$.

R^* is the critical particle radius, which is the size of the particle that is in equilibrium with the surrounding adatom concentration and consequently neither grows nor shrinks due to Ostwald ripening. Equation 11 can be rewritten for two limiting cases, namely, interface control with slow detachment or attachment of atoms at the surface of metal particles ($Y \gg X$) and diffusion control ($X \gg Y$). Depending on interface control or diffusion control, the critical radius, R^*, would be different. A rigorous definition for both can be found in recent work.[66]

For a metal particle of radius R less than the critical radius R^*, corresponding chemical potential $\Delta\mu_{NP}(R)$ is higher than that of R^*. dR/dt is negative, the metal atoms leave the metal particles to add to the support, and the metal particle size decreases. For the metal particles of the radius R larger than R^*, dR/dt becomes positive, the metal atoms leave the support to add to the metal particles, and the metal particle size increases. Thus, it is the difference of $\Delta\mu_{NP}$ between the metal particles of the radius R and critical radius R^* that determines the growth direction of the individual particle of interest and the overall evolution of the size distribution. R^* is sensitive to the size and spatial distribution of the metal particles, and would increase gradually with time. Under extreme cases where the metal particles have identical size and distribute homogeneously, there will be no difference of $\Delta\mu_{NP}$ between any metal particles on the support. This leads to a zero net flux of monomers, and Ostwald ripening will be completely suppressed, as indeed found in recent experiments.[67] The size for each individual metal particle will neither increase nor decrease, unless the sintering could proceed through the diffusion coalescence.

On the other hand, dR/dt also depends exponentially on the total activation energy E_{tot}, the sum of the formation energy of the adatoms E^{f}_{ma} and its diffusion barrier E^{d}_{ma}, which both are determined by the intrinsic interaction between the metal adatom and support. Since the metal adatoms on the support are often coordinate unsaturated, E^{f}_{ma} is usually highly endothermic and its absolute value is much larger than the chemical potential $\Delta\mu_{NP}$ of the metal particles. Without considering the contribution of the diffusion barrier E^{d}_{ma}, this already tells that the absolute time rate dR/dt would be dominated by the total activation energy. For a given metal catalyst, to suppress the Ostwald ripening rate, the optimized support should be the one with a higher total activation energy, which could be achieved by modifying or choosing different supports.

The kinetics discussed so far is based on the mean-field approximation, assuming the metal particles are well separated and in equilibrium with far field monomer. However, its applicability has been subject to much debate, and the mean-field approximation may even break down.[25,46,47,56,68−72] For instance, the long-range equilibrium may not be reached because of the presence of the defects and large diffusion barrier, a fact of that may lead to gradients in monomer concentration and thus to local effects. The local effect could be introduced in addition by the difference in size and spatial distribution of the metal particles in local vicinity, or a higher metal loading. In this case, the spatial separation of the metal particles could approach the diffusion length, L, and the particles could alter the concentration of monomers in the vicinity of neighboring particles. These may deviate simulated decay or growth of the metal particles based on the mean-field approximation from the measurement. To account for these effects, one should employ the so-called nearest neighbor approach or local correlation approach.[25,47,69−72] In this approach, the sintering of a metal particle of interest will be decided by its neighbor particles, and a local concentration $c_s^*(R)$ or critical radius R^* varying with spatial and size distribution of neighbor metal particles in the local vicinity should be defined and introduced in the above kinetic equations.

dx.doi.org/10.1021/ja3087054 | J. Am. Chem. Soc. 2013, 135, 1760−1771

2.3. Reactant Assisted Ostwald Ripening. Under the reaction conditions, the metal adatoms detached from the metal particles may be stabilized by reactants forming metal−reactant complexes as indicated in Figure 2b, and the concentration of the metal−reactant complexes as monomers will increase. This would promote Ostwald ripening of the metal particles and influence corresponding sintering behavior. To see when and how reactants assist Ostwald ripening and take advantage of the structural simplicity of the mononuclear metal−carbonyl complexes, we consider the supported metal particle under CO. The theory can, however, be extended easily to the multinuclear complexes and different reactant gases.

To stabilize a metal adatom, reactants should be able to form a chemical bond with the metal adatom, and corresponding binding energy $\overline{E}_{CO}^{ad}$ must be negative.

$$\overline{E}_{CO}^{ad} = E_{carb/ox} - E_{ma/ox} - n \times E_{CO} \tag{13}$$

where n is the number of CO coordinated to the metal adatom, $E_{carb/ox}$ is the total energy of the metal−carbonyl complexes on support, $E_{ma/ox}$ is the total energy of the metal adatom on support, and E_{CO} is the total energy of CO in gas phase. It is evident that the strong interaction between the reactant and the metal adatom is essential for the formation of the favorable chemical bond. Meanwhile, the local coordination and charge state of the metal adatom is sensitive to the support, which would influence the interaction between the metal adatom and the reactant. Hence, given a reactant and metal catalyst of interest, the overall binding strength between the reactant and the metal adatom could be mediated or tuned by modifying and choosing different supports.

For adsorption of reactants, loss of gas phase entropy should be taken into account. Accordingly, the Gibbs free energy of adsorption ΔG_{CO} should be used

$$\Delta G_{CO}(T, P) = \overline{E}_{CO}^{ad} - n \times \Delta\mu_{CO}(T, P) \tag{14}$$

If the chemical potential of reactants $\Delta\mu_{CO}$ is too low (low P or high T), the energy gain from the formation of the chemical bond cannot compensate the loss of gas-phase entropy. The corresponding adsorption would be endothermic and ΔG_{CO} is positive. For an exothermic adsorption ($\Delta G_{CO} < 0$), higher $\Delta\mu_{CO}$ is required and must satisfy the following condition

$$\Delta\mu_{CO}(ad) \geq \frac{1}{n}\overline{E}_{CO}^{ad} \tag{15}$$

The stabilization of the metal adatoms by adsorption of reactants would lower the formation energy of the metal adatoms by the amount of ΔG_{CO}. Corresponding concentration $\overline{c}_s(R)$ of monomers in the form of the metal−reactant complexes is

$$\overline{c}_s(R) = c_s^{eq} \exp\left[\frac{\Delta\overline{\mu}_{NP}(R)}{kT}\right] \exp\left[\frac{-\Delta G_{CO}}{kT}\right] \tag{16}$$

Compared to $c_s(R)$ for the metal adatoms in the absence of reactants (eq 10, a function of $\Delta\mu_{NP}(R)$ only), $\overline{c}_s(R)$ becomes a function of both $\Delta\overline{\mu}_{NP}(R)$ and $\Delta G_{CO}(T,P)$. For reactants interacting strongly with supported metal particles and the metal adatoms, both could be stabilized. Since the adsorption on supported metal particles occurs only at the exposed surface, the extent of stabilization over the particle by the amount of $\Delta\overline{\mu}_{NP} - \Delta\mu_{NP}$ would be much smaller than that of the individual metal adatoms by the amount of $-\Delta G_{CO}(T,P)$. As a result, the concentration of the metal-reactant complexes would increase exponentially and become the dominant monomers with respect to the metal adatoms when $\Delta G_{CO} < 0$.

The increase of concentration of monomers would affect the sintering kinetics. The corresponding time rate $d\overline{R}/dt$ of the supported metal particles in the presence of reactants via monomers in the form of the metal−reactant complexes becomes

$$\frac{d\overline{R}}{dt} = \frac{X\overline{Y}}{X+\overline{Y}}\frac{\overline{K}}{R^2}\exp\left[\frac{-\overline{E}_{tot}}{kT}\right]\left(\exp\left[\frac{\Delta\overline{\mu}_{NP}(R^*)}{kT}\right] - \exp\left[\frac{\Delta\overline{\mu}_{NP}(R)}{kT}\right]\right) \tag{17}$$

and $\overline{E}_{tot}$ is corresponding total activation energy

$$\overline{E}_{tot} = E_{carb}^{d} + E_{ma}^{f} + \Delta G_{CO} \tag{18}$$

where E_{carb}^{d} is the diffusion barrier of the metal−carboxyl complexes on support. It is clearly seen that the total activation energy becomes a function of the reaction conditions.

To see the influence of reactants on the kinetics, we note that, similar to the kinetics in the absence of reactants, the difference of the chemical potential $\Delta\overline{\mu}_{NP}$ of the metal particles between R^* and R determines the decay or growth direction, whereas the total activation energy $\overline{E}_{tot}$ dominates the absolute sintering rate. For reactant-assisted Ostwald ripening, corresponding total activation energy must be lower than that of the metal adatoms as monomers in the absence of reactants, namely

$$\overline{E}_{tot} < E_{tot} \tag{19}$$

Considering eq 18 and eq 12, this means

$$E_{carb}^{d} + \Delta G_{CO} < E_{ma}^{d} \tag{20}$$

For an exothermic adsorption ($\Delta G_{CO} < 0$), the concentration of monomers increases exponentially, and the total activation energy would decrease by ΔG_{CO}. However, the sintering rate may not necessarily increase unless eqs 19 and 20 are met. Actually, $\overline{E}_{tot}$ might be larger than E_{tot} if the corresponding diffusion barrier E_{carb}^{d} increases to such a value that even counteracts the gain of ΔG_{CO}, namely, $E_{carb}^{d} + \Delta G_{CO} > E_{ma}^{d}$. We note that the reduction of the formation energy and diffusion barrier E_{carb}^{d} of the metal−reactant complexes could both lead to a smaller $\overline{E}_{tot}$. Their relative values may be very different and even reversed compared to that of the metal adatom as monomers in the absence of reactants. This may have impact on Ostwald ripening. For instance, for the diffusion-controlled Ostwald ripening in the absence of reactants, if the metal−reactant complex formed in the presence of reactants has lower E_{carb}^{d}, the Ostwald ripening could switch to the interface control, and vice versa. For TiO_2(110)-supported Au particles at a diameter of 3 nm, Campbell and co-workers estimated that corresponding total activation energy in ultrahigh vacuum was 280 kJ/mol,[11] whereas under CO oxidation condition, Goodman and co-workers found that corresponding activation energy was about 10 ± 2 kJ/mol only.[25] Though the reason for the different activation energies is unclear, the dramatic influence of the reaction conditions on sintering is evident. This highlights the importance of the *in situ* study on the sintering kinetics, as well documented in the literature.[26,46,47,74]

dx.doi.org/10.1021/ja3087054 | J. Am. Chem. Soc. 2013, 135, 1760−1771

2.4. Reactant Induced Disintegration. Apart from reactant-assisted Ostwald ripening via the metal−reactant complexes as a transient monomer whose formation should be prevented, reactants could disintegrate supported metal particles into the individual complexes as the final product spreading out on support. This is likely when the metal−reactant bond energy exceeds the difference in energy between the metal−metal and metal−support bonds.[48,49] Since a fact of this could be used to regenerate or redisperse the low surface area catalysts, the formation of the metal−reactant complexes should be maximized. A rigorous thermodynamic study on this topic is described here.

For reactant induced disintegration of a metal particle of the radius R to the individual metal−reactant complexes, the Gibbs free energy of adsorption of reactants on the metal adatoms should be low enough to compensate the cost of the formation energy of the metal adatom with respect to the metal particle of interest. The feasibility could be described by the Gibbs free energy of disintegration, ΔG_{NP}^{dis}, of the NP into the metal−reactant complexes using CO as an example again

$$\Delta G_{NP}^{dis}(R, T, P) = \Delta G_{CO}(T, P) + E_{ma}^{f} - \Delta \bar{E}_{NP}(R) - TS \quad (21)$$

where S is the configurational entropy[75] of the complexes disintegrated from the metal particle of interest.

To disintegrate a supported metal particle, corresponding ΔG_{NP}^{dis} must be exothermic (negative). Considering eq 9, eq 13, and eq 14, the formula can be reformulated as

$$\Delta G_{NP}^{dis}(R, T, P) = E_{carb}^{f} - n \times \Delta\mu_{CO}(T, P) - \Delta \bar{E}_{NP}(R) - TS \quad (22)$$

where $E_{carb}^{f} = \bar{E}_{CO}^{ad} + E_{ma}^{f}$ is the formation energy of the metal−reactant complexes on support with respect to the infinite size metal particle and reactants in gas phase. It can be found that the overall value of ΔG_{NP}^{dis} is decided by four parts, namely, the formation energy of the complexes, the (average) energetics of the metal particles, the chemical potential of reactants in gas phase, and the configuration entropy due to the disintegration. Their influence and implication are discussed below.

First, a lower formation energy E_{carb}^{f} would lead a lower ΔG_{NP}^{dis}. For a given metal catalyst and support, this could be achieved by varying the composition of reactant gases, which interacts strongly with the metal adatoms. When the metal catalyst and support change, the reactant gas should change accordingly for favorable disintegration, since E_{carb}^{f} is determined by the overall interaction between the reactant, metal, and support. This is indeed corroborated by a number of experiments. To disperse the metal catalysts in experiment, the calcination in oxidizing conditions is widely used: depending on the catalysts and supports, different oxidizing reactants had been adopted.[27,51−55]

Second, ΔG_{NP}^{dis} is also sensitive to the reaction conditions and the size of the metal particles. For a given metal particle of the radius R, corresponding chemical potential $\Delta\mu_{CO}(\mathrm{dis})$ of reactants necessary for disintegration ($\Delta G_{NP}^{dis} \le 0$) is

$$\Delta\mu_{CO}(\mathrm{dis}) \ge \frac{1}{n}(E_{carb}^{f} - \Delta \bar{E}_{NP}(R) - TS) \quad (23)$$

It is clear that higher chemical potential of reactants (higher P and/or lower T) will be required for the complexes with higher formation energy and the particle with lower chemical potential. Under a given reaction condition $\Delta\mu_{CO}$, the metal particles of the radius less than $R(\mathrm{dis})$ by considering eq 2 will be disintegrated

$$R(\mathrm{dis}) \le 3\Omega\bar{\gamma}_{me}(E_{carb}^{f} - n \times \Delta\mu_{CO}(T, P) - TS)^{-1} \quad (24)$$

It is worth to note that the above criterion for the reactant induced disintegration of a particle of interest is rather different from that of the exothermic adsorption of reactant on adatoms defined by eq 15. This can be seen from the difference of corresponding chemical potential required between eqs 15 and 23

$$\Delta\mu_{CO}(\mathrm{dis}) - \Delta\mu_{CO}(\mathrm{ad}) = \frac{1}{n}(E_{ma}^{f} - \Delta \bar{E}_{NP}(R) - TS) \quad (25)$$

Since the energetics of the metal adatoms on support (E_{ma}^{f}) is usually much higher than that of supported metal particles ($\Delta \bar{E}_{NP}$), the difference would be rather positive. In other words, much higher chemical potential of reactant would be required for disintegration. To regenerate the metal catalysts from the disintegrated complexes, one should lower the chemical potential of reactants (increase T, decrease P, or apply at same time) to decompose the complexes. By controlling the reducing conditions (T and P) and time, the metal adatoms released could start to agglomerate and form cluster until the desired size of the metal particles (thus redispersion) is reached.

3. TiO_2(110) SUPPORTED RH PARTICLES UNDER CO

3.1. Energetics. The formalism developed above was applied to TiO_2(110) supported Rh particles under CO, because of its importance in CO hydrogenation and a lot of experimental studies available for comparison.[35−40] Most energetics required are calculated using vienna ab initio simulation package (VASP)[76] unless mentioned otherwise (see details in Supporting Information). Important data are given in Table 1. Formation energy E_{ma}^{f} of Rh adatom on TiO_2(110) at the most stable site is highly endothermic by 2.85 eV. This means a rather low concentration of Rh adatom as monomers on TiO_2(110) and high activation energy of sintering for supported Rh particles in ultrahigh vacuum. CO interacts strongly with Rh adatom on top with binding energy $\bar{E}_{CO}^{ad}$ of −2.18 eV to form monocarbonyl complexes, as shown in Figure 3. The second CO can adsorb on Rh adatoms to form dicarbonyl complexes with overall binding energy of −4.29 eV. Corresponding formation energy E_{carb}^{f} of Rh carbonyls with

Table 1. Calculated Molar Volume Ω (Å^3) of Bulk Rh atom, Formation Energy of Rh Adatom E_{ma}^{f}, Binding Energy of CO on Rh Adatom $\bar{E}_{CO}^{ad}$, and Formation Energy of the Rh Carbonyl Complexes E_{carb}^{f} for the Monocarbonyl and Dicarbonyl Complexes on TiO_2(110)[a]

	Rh
Ω	14.38
E_{ma}^{f}	2.85
$\bar{E}_{CO}^{ad}$ (mono)	−2.18
$\bar{E}_{CO}^{ad}$ (di)	−4.29
E_{carb}^{f} (mono)	0.67
E_{carb}^{f} (di)	−1.44

[a]Energy Unit is eV.

dx.doi.org/10.1021/ja3087054 | J. Am. Chem. Soc. 2013, 135, 1760−1771

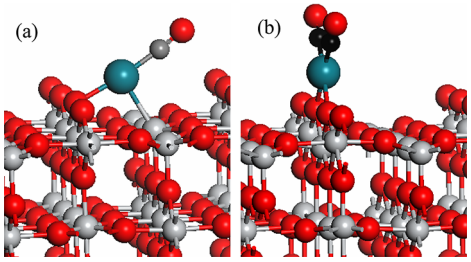

Figure 3. Optimized most stable structures of the Rh carbonyls on $TiO_2(110)$. The Rh of Rh(CO) sits at the hollow site coordinating with one bridge O and one fivefold Ti_{5f}. The Rh of $Rh(CO)_2$ sits at the bridge site between the two bridging O. Red: O, gray: Ti, cyan: Rh, black: C.

respect to bulk Rh are 0.67 and −1.44 eV for the monocarbonyl and the dicarbonyl complexes, respectively. The strong binding between CO and Rh as well as the negative formation energy for the dicarbonyl complexes implies that the presence of CO would have significant influence on the sintering and disintegration, which will be discussed in detail below based on calculated Gibbs free energy.

3.2. Surface Energy. For the surface energy, γ_{me}, of Rh, various orientations including (111), (110), (100), (210), (211), (221), (310), and (311) were considered. Based on the surface energies calculated and Wulff construction, the equilibrium morphology of infinite size Rh particle is obtained and shown in Figure 4a. The exposed facets, corresponding

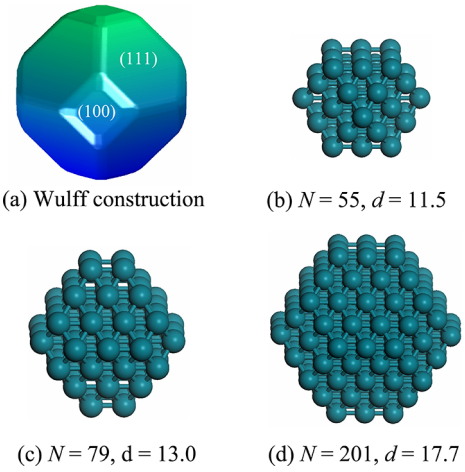

Figure 4. (a) Infinite size Rh morphology from Wulff construction based on the surface energies calculated by first-principles theory. Optimized cuboctahedral Rh particles based on Wulff construction containing 55 (b), 79 (c), and 201 (d) Rh atoms, and corresponding diameters d are 11.5, 13.0, and 17.7 Å.

surface energies and ratio, are given in Table 2. It is found that (111), (311), and (100) facets cover 71%, 9%, and 7% area exposed, respectively. The average surface energy over the equilibrium morphology is 0.119 eV/Å^2. The similar surface energy between the average surface and the (111) surface (less than 6 meV/Å^2) comes from the small difference of surface energies between various facets exposed, and a higher ratio of (111) surface. The average surface energies calculated agrees well with the measured surface energy (0.125 eV/Å^2) of liquid Rh.[77]

Table 2. Calculated Surface Energies γ_i and Ratio f_i of Exposed Facets of Infinite Size Rh based on Wulff Construction[a]

facet	γ_i (eV/Å^2)	f_i(%)
(111)	0.113	71
(311)	0.136	9
(100)	0.136	7
(221)	0.127	6
(211)	0.131	4
(310)	0.140	3
γ_{me}	0.119	
Exp.	0.125	

[a]Calculated Average Surface Energy over Wulff Construction γ_{me} and Experimental Value of Liquid Rh.[77].

To see the influence of CO adsorption on $\Delta\gamma_{me}$ (eq 5), we considered CO adsorption on Rh(111). First, the average binding energies, E_{CO}^{ad}, from coverage of 1/16 ML to 12/16 ML were calculated. In view of experimental results,[78] the CO adsorption was calculated at top site when CO coverage θ is below 0.25 ML, and at top+hollow sites when θ > 0.25 ML (see Figure S1 in SI). The calculated result is shown in Figure 5.

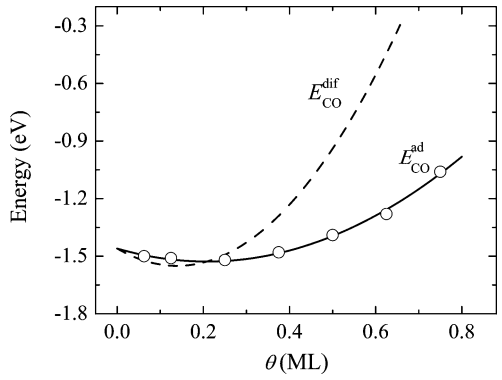

Figure 5. Calculated average binding energy E_{CO}^{ab} (circle) of CO on Rh(111) versus CO coverage. The result is fitted to a quadratic polynomial, $E_{CO}^{ab} = -1.46 - 0.65\theta + 1.56\theta^2$, and plotted by a solid line for convenience of the interpolation. The dashed line is the differential binding energy, $E_{CO}^{dif} = -1.46 - 1.31\theta + 4.67\theta^2$.

From the average binding energy, the differential binding energy E_{CO}^{dif} of CO is obtained, and plotted in Figure 5 too. The coverage θ of CO adsorbed on Rh(111) versus chemical potential of CO in gas phase can therefore be calculated by eq 6, and plotted in Figure 6a. Based on these, the reduction of surface energy $\Delta\gamma_{me}^{(111)}$ on Rh(111) due to the adsorption of CO is obtained and plotted in Figure 6b. It can be found that, when $\Delta\mu_{CO}$ is lower than −1.52 eV, there is no CO adsorption on Rh(111), and no change in surface energy. With increasing $\Delta\mu_{CO}$, CO starts to adsorb and corresponding coverage increases. Accordingly, the reduction of surface energy $\Delta\gamma_{me}^{(111)}$ increases monotonically. Under typical experimental conditions of 300 K and 10^{-1} mbar ($\Delta\mu_{CO}$ = −0.76 eV), corresponding $\Delta\gamma_{me}^{(111)}$ is as large as −0.050 eV/Å^2. In comparison to the surface energy of bare Rh(111) γ_{me} = 0.119 eV/Å^2, the great influence of the adsorption of reactants on surface energy is clearly seen.

3.3. Chemical Potential. Using the surface energy of infinite-size Rh particle, chemical potential $\Delta\mu_{NP}$ of the free-standing Rh particles (eq 4) versus the diameter $d = 2R$ was

dx.doi.org/10.1021/ja3087054 | J. Am. Chem. Soc. 2013, 135, 1760−1771

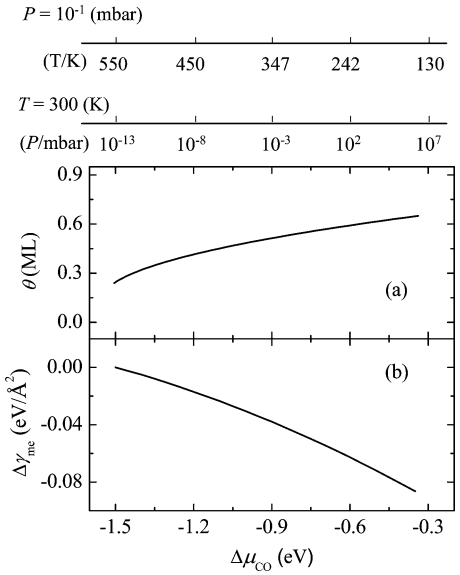

Figure 6. (a) Calculated CO coverage θ (ML) on Rh(111) versus chemical potential $\Delta\mu_{CO}$ of CO in gas phase. (b) Reduction of surface energy $\Delta\gamma_{me}$ of Rh(111) due to CO adsorption, and the fitted quadratic polynomial is $\Delta\gamma_{me}^{(111)} = -0.124 - 0.115\Delta\mu_{CO} - 0.0215\Delta\mu_{CO}^2$ for convenience of the interpolation. The relation between $\Delta\mu_{CO}$ and T at 10^{-1} mbar and P at T = 300 K is indicated in the top panel.

calculated and plotted in Figure 7. The average energy ΔE_{NP} (eq 2), which is a factor of $1^1/_2$ larger than that of $\Delta\mu_{NP}$, is also

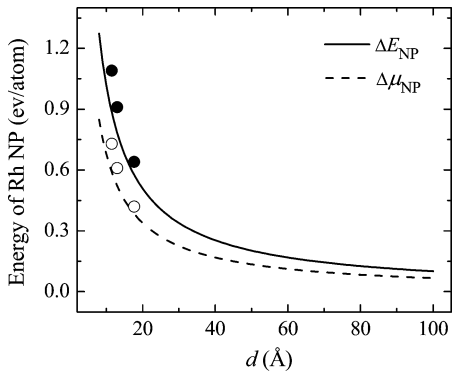

Figure 7. Chemical potential $\Delta\mu_{NP}$ (dashed line) and average energy E_{NP} (solid line) of free-standing Rh particle in the absence of reactants versus the diameter d. The surface energy used is the average surface energy of infinite-size Rh based on Wulff construction. The open and solid circles are calculated energies of Rh particles (see Figure 4). The zero reference is infinite-size Rh.

plotted for reference. It can be found that, with decrease of d from 100 to 50 Å, $\Delta\mu_{NP}$ increases slowly up to 0.14 eV with respect to infinite-size Rh. Further decrease of d will lead to a rapid increase of $\Delta\mu_{NP}(d)$, for instance, 0.23 eV at 30 Å and 0.68 eV at 10 Å.

It was reported that chemical potential of supported metal particles at small size was underestimated if the size-independent surface energy is used in the $G-T$ relation (eq 4).[11,56] The high ratio of the coordinate-unsaturated atoms exposed at small size would increase the surface energy and make it size dependent. To see the size effect on the surface energy and chemical potential of Rh particles considered here, we constructed three cuboctahedral Rh nanoparticles including N = 55, 79, and 201 atoms as plotted in Figure 4b,c,d based on above Wulff construction of infinite-size Rh. Effective diameters $d = 2R$ calculated by $V = N\Omega = 4\pi R^3/3$ are 11.5, 13.0, and 17.7 Å, respectively. The three Rh nanoparticles were fully relaxed. The average energies calculated with respect to infinite size Rh (ΔE_{NP}) are 1.09 (N = 55), 0.91 (N = 79), and 0.64 (N = 201) eV/Rh atom, and the corresponding chemical potentials $\Delta\mu_{NP}$ are 0.73, 0.61, and 0.42 eV/Rh atom, which all are included in Figure 7. For comparison, corresponding chemical potentials from the $G-T$ relation, using the surface energy of infinite-size Rh, are 0.60, 0.53, and 0.39 eV. Although the result based on the $G-T$ relation are indeed underestimated, the difference is only 0.13 eV/Rh atom for the smallest Rh nanoparticle (d = 11.5 Å) considered. For the Rh nanoparticle of d = 17.7 Å, the difference already falls to 0.03 eV/Rh atom. This indicates that, for Rh particles considered here, the size effect on the surface energy and chemical potential is modest. To rationalize this result, we note that the optimized surface in-plane lattice constants of Rh particles are found to decrease on average by about 0.08 Å (3% lateral contraction), compared to the bulk truncated one. It is likely that, at small particle size, the decrease of the surface energy from the smaller in-plane lattice constant compensates the increase of the surface energy from the higher ratio of the coordinate-unsaturated atoms exposed.

For Rh particles under CO that can adsorb, corresponding chemical potential $\Delta\bar{\mu}_{NP}$ becomes a function of both the diameter d and chemical potential $\Delta\mu_{CO}$ of CO. For CO adsorption, one should in principle consider all possible facets exposed. The procedure would be rather tedious, since under different $\Delta\mu_{CO}$, adsorption configuration could be different and vary further on different facets. All these would change corresponding morphology. This may be more involved by considering the possible size effect upon CO adsorption. As an approximation, we considered only Rh(111), thus neglecting all other facets exposed. This approximation is rationalized by a so-called compensation effect. First, though the different facets may interact differently with CO, the facets with higher surface energy would bind more strongly with CO. Second, although the smaller particles may interact differently with CO, the smaller particle with a higher ratio of coordinate-unsaturated metal atoms would also bind more strongly with CO. Actually, as indicated above, the surface energy of Rh(111) is close to the average one from Wulff construction, and the size effect on the chemical potential of free-standing Rh particles is also small. The validity of the approximation is justified finally by the nice agreement of CO induced disintegration of Rh at the broad T, P, and d range as discussed below.

Before presenting chemical potential of supported Rh particles under CO for following application, we note that in experiment the size of supported particles is usually measured by the diameter d of the projection of the particle of the radius R on support, as indicated in Figure 1. To compare with experiment, the d instead of R is used in the following without mention otherwise. Considering the contact angle α, the relation between d and R is as follows: when $0 < \alpha \leq \pi/2$, $d = 2R \sin(\alpha)$, and when $\pi/2 \leq \alpha \leq \pi$, $d = 2R$. For TiO_2(110) supported Rh particles, the contact angle α can be estimated from the experiment,[37] where the height/diameter ratio of supported Rh particles was approximately 0.3 at the coverages considered. Corresponding contact angle α is estimated to be $\pi/3$, and $R = d/\sqrt{3}$.

dx.doi.org/10.1021/ja3087054 | J. Am. Chem. Soc. 2013, 135, 1760−1771

The resulted $\Delta\overline{\mu}_{NP}$ versus the reciprocal of d and $\Delta\mu_{CO}$ is plotted in Figure 8. Under a given $\Delta\mu_{CO}$, $\Delta\overline{\mu}_{NP}$ increases

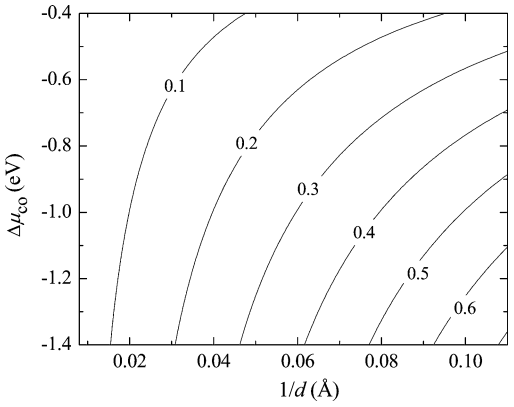

Figure 8. Contour plot of chemical potential $\Delta\overline{\mu}_{NP}$ of $TiO_2(110)$ supported Rh particles versus the chemical potential $\Delta\mu_{CO}$ and the reciprocal of the diameter d. The contact angle $\alpha = \pi/3$ estimated from the experiment[37] was used here and in the following figures without mention otherwise.

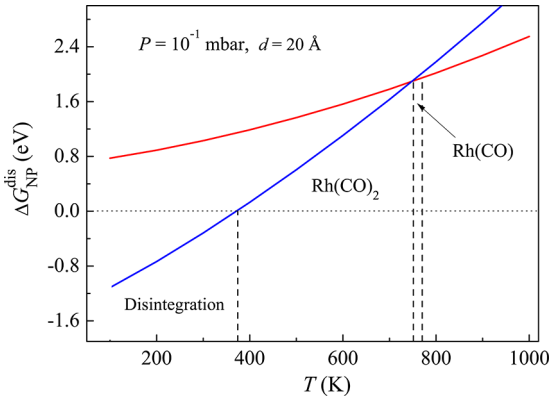

Figure 9. Temperature dependence of the Gibbs free energy of disintegration ΔG^{dis}_{NP} of the metal−reactant complexes of Rh(CO) (red solid line) and $Rh(CO)_2$ (blue solid line) with respect to $TiO_2(110)$ supported Rh particle of the diameter d = 20 Å under 10^{-1} mbar CO. The vertical dashed lines from right to left represent the temperature boundary for which Rh(CO) and $Rh(CO)_2$ complexes becomes the dominated monomers, and the supported Rh NP of interest is disintegrated into $Rh(CO)_2$, respectively.

linearly with the reciprocal of d, as expected. Whereas under a given d, $\Delta\overline{\mu}_{NP}$ decreases monotonically with increase of $\Delta\mu_{CO}$. Namely, supported Rh particles would be stabilized gradually with increase of chemical potential of CO (higher P or lower T) due to the adsorption of CO, which is not surprising at all. Interestingly, larger Rh particles under lower $\Delta\mu_{CO}$ could have the same chemical potential as those of smaller ones under higher $\Delta\mu_{CO}$, which manifests again the stabilization of reactants. Pronounced influence of reactants on chemical potential of supported metal particles would affect the sintering rate, as found in recent experiments.[60] Its interplay with the stabilization of the metal adatoms would determine the overall effect of reactants on sintering and disintegration.

3.4. Gibbs Free Energy of Disintegration. Based on the above energetics, the influence of T and P of CO on sintering and disintegration of supported metal particles at given size was studied first. In the experiment,[37] the diameter of Rh particles on $TiO_2(110)$ as prepared at the submonolayer regime of Θ = 0.01 ML falls in the range of 10−20 Å, and increased slightly at 0.05 ML. Considering the limitation of the present theory and experimental error bar at small radius, we set the particles of the diameter d = 20 Å in calculation. The configuration entropy S of the formation of the individual complexes due to the disintegration of Rh particles at Θ = 0.01 ML is 4.83×10^{-4}, and should be taken into account. Corresponding Gibbs free energy of disintegration $\Delta G^{dis}_{NP}(T, P)$ of the Rh carbonyl complexes was parametrized accordingly

$$\Delta G^{dis}_{NP}(T, P) = E^{f}_{carb} - n \times \Delta\mu_{CO}(T, P) - 3.74\overline{\gamma}_{me}(T, P) - 4.83 \times 10^{-4}T \quad (26)$$

where n = 1 represents for the monocarbonyl Rh(CO) and n = 2 for the dicarbonyl $Rh(CO)_2$.

The dependence of $\Delta G^{dis}_{NP}(T,P)$ on T was studied at experimental condition of $P = 10^{-1}$ mbar.[37] Calculated ΔG^{dis}_{NP} for both Rh(CO) and $Rh(CO)_2$ are shown in Figure 9 for T in the range 100−1000 K. It can be found that calculated ΔG^{dis}_{NP} decreases almost linearly with decrease of T, namely, lower T (higher $\Delta\mu_{CO}$) favors the formation of the Rh carbonyl complexes. Meanwhile, formation of $Rh(CO)_2$ complexes becomes energetically favorable when T < 750 K because of relatively lower ΔG^{dis}_{NP}. Accidentally, CO starts to adsorb on Rh particles since the corresponding $\Delta\mu_{CO} > -1.52$ eV (Figure 6b). To be exothermic adsorption of CO on Rh adatoms (criterion defined by eq 15), the corresponding $\Delta\mu_{CO}$ must be higher than −2.18 eV ($T \leq 770$ K at $P = 10^{-1}$ mbar) for Rh(CO), and −2.15 eV ($T \leq 760$ K) for $Rh(CO)_2$. Considering ΔG^{dis}_{NP} for Rh(CO) and $Rh(CO)_2$ cross at 750 K, this says that Rh(CO) complexes instead of the metal adatoms will become the dominant monomers for T in the range of [750, 770] K, whereas the dominant complexes will become $Rh(CO)_2$ for T in the range of [370, 750] K. Once the diffusivity and barrier of the monomers (the metal adatoms and the metal−reactant complexes) are available, the corresponding total activation energies E_{tot} and $\overline{E}_{tot}$ can be calculated. Whether Ostwald ripening will be assisted by CO could be justified by eqs 19 and 20. When $T \leq 370$ K, the corresponding ΔG^{dis}_{NP} crosses the zero reference, criterion defined by eq 23 is satisfied. Rh particles of d = 20 Å will be disintegrated to the individual $Rh(CO)_2$, in the case of no kinetics hindrance.

Now, we turn to the influence of P on sintering and disintegration at experimental conditions of T = 300 K,[37] and the calculated $\Delta G^{dis}_{NP}(T, P)$ is plotted in Figure 10. It can be found that ΔG^{dis}_{NP} for both Rh(CO) and $Rh(CO)_2$ decrease almost linearly with increase of lg(P). Higher P would favor the formation of the metal−carbonyl complexes. Similar to above, one can find that, for P in the range of $[10^{-25}, 10^{-24}]$ mbar which could occur at most experimental conditions, Rh(CO) instead of the metal adatoms will become the dominant monomers, whereas for P in the range of $[10^{-24}, 10^{-4}]$ mbar, dominant complexes will become $Rh(CO)_2$. When $P > 10^{-4}$ mbar, ΔG^{dis}_{NP} crosses the zero reference and becomes negative. Accordingly, Rh particles of d = 20 Å will be disintegrated to the individual $Rh(CO)_2$.

To see the size dependence of the disintegration induced by CO, T and P are fixed at the experimental condition of 300 K and 10^{-1} mbar.[37] Under these conditions ($\Delta\mu_{CO}$ = −0.76 eV) according to Figure 6, the reduction of the surface energy of Rh particles due to CO adsorption is 0.050 eV/Å^2, and the effective surface energy $\overline{\gamma}_{me}$ becomes 0.069 eV/Å^2, which is much smaller

dx.doi.org/10.1021/ja3087054 | J. Am. Chem. Soc. 2013, 135, 1760−1771

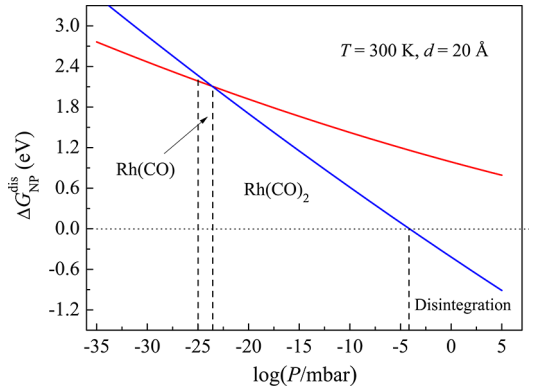

Figure 10. Pressure dependence of the Gibbs free energy of disintegration ΔG_{NP}^{dis} of the metal−reactant complexes of Rh(CO) (red solid line) and $Rh(CO)_2$ (blue solid line) with respect to $TiO_2(110)$ supported Rh particle of the diameter d = 20 Å at T = 300 K. The vertical dashed lines from left to right represent the pressure boundary for which Rh(CO) and $Rh(CO)_2$ complexes becomes the dominated monomers, and the supported Rh NP of interest is disintegrated into $Rh(CO)_2$, respectively.

than that of the bare bulk (0.119 eV/Å^2). On the other hand, the formation of $Rh(CO)_2$ is thermodynamically more favorable than that of Rh(CO) at this particular condition. Corresponding ΔG_{NP}^{dis} for $Rh(CO)_2$ versus d was parametrized and became only the function of d.

$$\Delta G_{NP}^{dis}(d) = 0.08 - 5.16/d \quad (27)$$

The calculated result is plotted in Figure 11. It can be found that ΔG_{NP}^{dis} decreases with decrease of d and crosses the zero

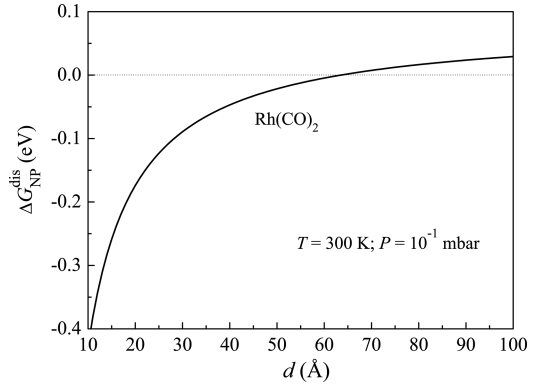

Figure 11. Size dependence of the Gibbs free energy of disintegration ΔG_{NP}^{dis} of the metal−reactant complexes of $Rh(CO)_2$ with respect to $TiO_2(110)$ supported Rh particle under 10^{-1} mbar CO at T = 300 K.

reference at about 60 Å. This tells that Rh particles of the diameter less than this would be disintegrated into $Rh(CO)_2$ at T = 300 K and $P = 10^{-1}$ mbar. With further decrease of the size, the rate of the disintegration would increase due to the dramatic drop of ΔG_{NP}^{dis} providing an even larger driven force.

3.5. Discussion. The results above reproduce well the broad T, P, and d range over which the sintering and disintegration occurred in such experiments even on different supports.[35−40] For $TiO_2(110)$ supported Rh particles as prepared at d in the range 10−20 Å,[37] the size decrease was indeed observed at $P = 10^{-3}$ mbar and 300 K. As seen from Figure 10, $P = 10^{-3}$ mbar falls in the pressure window of disintegration ($P > 10^{-4}$ mbar). With gradual increase of P up to 10^{-1} mbar, the experiment found that the rate of the disruption of supported Rh particles as prepared increases rapidly, and disappeared completely with time. This is understandable because corresponding pressure falls well in the pressure window for disintegration according to above calculation. In a time-resolved in situ Fourier transformed infrared adsorption spectroscopy (FT-IR) study of Al_2O_3-supported Rh particles (298 K and 26.7 kPa),[38] the Rh(CO) complex was found at the initial exposure of CO, but only the $Rh(CO)_2$ complex was observed under the extended exposure. This can be rationalized by the above calculations which predict that the $Rh(CO)_2$ complex is thermodynamically more favorable at the experimental conditions. It is likely that the kinetics hindrance of adsorbed CO attaching to the metastable Rh(CO) allows it to be observed by experiment. CO induced disintegration of Rh particles supported on planar SiO_2 was also studied by Goodman and co-workers using polarization modulation infrared adsorption spectroscopy (PM-IRAS).[40] For Rh particles of d = 16 Å on average, $Rh(CO)_2$ PM-IRAS signal was detected when $P > 10^{-5}$ mbar at 400 K. The increase of signal intensity with P also corroborates well with lower Gibbs free energy of formation of the complexes with P plotted in Figure 10.

STM experiment[37] found that disintegrated Rh species from the Rh particles of d = 10−20 Å on $TiO_2(110)$ at 10^{-1} mbar CO and 300 K started to agglomerate and form small Rh particles, when the samples was annealed up to 400 K under the same P. Experiments found further that, when annealing T was increased further to 600 K, the average diameter of the Rh particles attained a value of 55 Å. In contrast, without the pretreatment of CO, the Rh particles as prepared in the range 10−20 Å attained only the average diameter of 35 Å when the samples were annealed at 900 K under ultrahigh vacuum. As shown in Figure 9, when T is higher than 370 K at 10^{-1} mbar CO, ΔG_{NP}^{dis} becomes positive, and falls in the temperature window dominated by $Rh(CO)_2$ monomers. Since the concentration of the corresponding monomers is much higher than that of the metal adatoms in the absence of CO, agglomeration to the larger metal particles would be promoted.

In terms of the size effect, experiments[37] found that under 10^{-1} mbar CO and at 300 K, the Rh particles of d = 10−20 Å supported on $TiO_2(110)$ were rapidly disintegrated into atomically dispersed species, while the process was slow for those with d = 30−40 Å, and did not occur for those with d = 80−100 Å particles, even at higher P and extended exposure time. These experimental results are corroborated again by our result shown in Figure 11, which indicates that the Rh particles of the diameter less than ∼60 Å would be disintegrated by CO, whereas the larger one would be resistant to the disintegration. Similar size dependence of the disintegration by CO was also found on SiO_2 supported Rh particles.[40] In that work, the PM-IRAS intensity of the $Rh(CO)_2$ complexes disintegrated from the Rh particles of d = 16 Å was found at 10^{-1} mbar and 400 K, but no $Rh(CO)_2$ signal was detected for the Rh particles of d = 37 Å under same conditions.

Excellent agreement between theory and experiment over the broad range of temperature, pressure, and particle size justifies the theory developed and approximation of surface energy of supported Rh particles. This also shows that the formation of the metal−reactant complexes as favorable monomers plays a crucial role in the sintering and disintegration of supported metal particles under reaction conditions. Depending on the conditions, it could act not only as transient monomers to assist

dx.doi.org/10.1021/ja3087054 | J. Am. Chem. Soc. 2013, 135, 1760−1771

Ostwald ripening, but also as the final product of the disintegration. It is interesting to note that the calculations based on $TiO_2(110)$ could rationalize the experimental results of Rh disintegration on various supports. This indicates that the overall processes considered is less sensitive to the supports, which is understandable due to the strong interaction between CO and Rh. The mechanism presented could apply for various metal−oxide systems and chemical environments. For instance, NO molecules, which interacts strongly with transition metals,[79] could also induce the disintegration of supported Rh particles.[37] The formation of Rh-nitrosyl complexes was found in the reaction between NO and CO, and was suggested to be responsible for the observed redispersion.[24] For Pt interacting strongly with both CO and O_2, the presence of either of them was also found to influence the corresponding sintering and redispersion process.[46,47,80]

4. SUMMARY

We develop an atomistic theory of Ostwald ripening and disintegration of supported metal particles under reaction conditions. The influence of the adsorption of reactants on the surface energy and chemical potential of supported metal particles are well described. For reactant assisted Ostwald ripening and induced disintegration, the strong interaction between reactant and metal adatom is essential. Corresponding thermodynamic criteria and the Ostwald ripening rate equation are derived. When the adsorption of reactants on the metal adatoms is exothermic, the metal−reactant complexes becomes the dominant monomers. If the total activation energy of the complexes as monomers is lower than that of the metal adatoms in the absence of reactants, Ostwald ripening will be promoted. When the formation of the complexes becomes exothermic with respect to the supported metal particles of interest, the metal particles will be disintegrated to the individual complexes. The disintegrated metal−reactant complexes could be subjected to further reduction for regeneration of the catalysts with desired dispersion.

A prominent feature of the theory developed is that most of the energetics and kinetics data required can be calculated conveniently by first-principles theory. These would allow for a rapid, quantitative, and systematic exploration of sintering and redispersion of supported metal particles in huge phase space of structures and compositions under various reaction environments. To suppress the Ostwald ripening rate under given reaction conditions, the support with higher total activation energies for both the metal adatoms and metal−reactant complexes are essential. The Ostwald ripening rate could be suppressed further by preparing the homogeneous distributed metal particles with identical size. To facilitate the disintegration and redisperse the low surface area catalysts, one should choose proper reactant gases and control reaction conditions (temperature and pressure) in such a way that the corresponding Gibbs free energy of disintegration becomes exothermic.

■ ASSOCIATED CONTENT

Supporting Information

Computational details, Figure S1, and the coordinates for the optimized structures considered. This material is available free of charge via the Internet at http://pubs.acs.org/.

■ AUTHOR INFORMATION

Corresponding Author

*E-mail: wxli@dicp.ac.cn

Notes

The authors declare no competing financial interest.

■ ACKNOWLEDGMENTS

We thank Dr. Fan Yang for fruitful discussion and Bryan Goldsmith for reading the manuscript carefully. This work was supported by the National Natural Science Foundation of China (20923001, 21173210, 21225315) and the National Basic Research Program of China (973 Program, 2013CB834603). Calculations were carried out at National Supercomputing Center in Tianjin, China.

■ REFERENCES

(1) Bell, A. T. *Science* **2003**, *299*, 1688.
(2) Hammer, B. *Phys. Rev. Lett.* **1999**, *83*, 3681.
(3) Dahl, S.; Logadottir, A.; Egeberg, R. C.; Larsen, J. H.; Chorkendorff, I.; Tornqvist, E.; Norskov, J. K. *Phys. Rev. Lett.* **1999**, *83*, 1814.
(4) Roduner, E. *Chem. Soc. Rev.* **2006**, *35*, 583.
(5) Cuenya, B. R. *Thin Solid Films* **2010**, *518*, 3127.
(6) Fu, Q.; Li, W. X.; Yao, Y. X.; Liu, H. Y.; Su, H. Y.; Ma, D.; Gu, X. K.; Chen, L. M.; Wang, Z.; Zhang, H.; Wang, B.; Bao, X. H. *Science* **2010**, *328*, 1141.
(7) Wynblatt, P.; Gjostein, N. A. *Acta Metall.* **1976**, *24*, 1165.
(8) Wynblatt, P.; Gjostein, N. A. In *Progress in Solid State Chemistry*, McCaldin, J. O., Somorjai, G. A., Eds.; Elsevier Science: Amsterdam, 1975; Vol. *9*; p 21.
(9) Kolmakov, A.; Goodman, D. W. *Chem. Rec.* **2002**, *2*, 446.
(10) Mitchell, C. E. J.; Howard, A.; Carney, M.; Egdell, R. G. *Surf. Sci.* **2001**, *490*, 196.
(11) Parker, S. C.; Campbell, C. T. *Phys. Rev. B* **2007**, *75*, 035430.
(12) Farmer, J. A.; Campbell, C. T. *Science* **2010**, *329*, 933.
(13) Shiju, N. R. *ChemCatChem* **2011**, *3*, 112.
(14) Li, Y.; Somorjai, G. A. *Nano Lett.* **2010**, *10*, 2289.
(15) Tao, F.; Salmeron, M. *Science* **2011**, *331*, 171.
(16) Freund, H.-J.; Kuhlenbeck, H.; Libuda, J.; Rupprechter, G.; Bäumer, M.; Hamann, H. *Top. Catal.* **2001**, *15*, 201.
(17) Newton, M. A. *Chem. Soc. Rev.* **2008**, *37*, 2644.
(18) Starr, D. E.; Shaikhutdinov, S. K.; Freund, H.-J. *Top. Catal.* **2005**, *36*, 33.
(19) Van't Blik, H. F. J.; Van Zon, J. B. A. D.; Huizinga, T.; Vis, J. C.; Koningsberger, D. C.; Prins, R. *J. Phys. Chem.* **1983**, *87*, 2264.
(20) Zaki, M. I.; Kunzmann, G.; Gates, B. C.; Knözinger, H. *J. Phys. Chem.* **1986**, *91*, 1486.
(21) Solymosi, F.; Bánsági, T. *J. Phys. Chem.* **1993**, *97*, 10133.
(22) Berkó, A.; Solymosi, F. *Surf. Sci. Lett.* **1998**, *411*, L900.
(23) Frank, M.; Kühnemuth, R.; Bäumer, M.; Freund, H.-J. *Surf. Sci.* **2000**, *454−456*, 968.
(24) Dent, A. J.; Evans, J.; Fiddy, S. G.; Jyoti, B.; Newton, M. A.; Tromp, M. *Angew. Chem., Int. Ed.* **2007**, *46*, 5356.
(25) Yang, F.; Chen, M. S.; Goodman, D. W. *J. Phys. Chem. C* **2009**, *113*, 254.
(26) Challa, S. R.; Delariva, A. R.; Hansen, T. W.; Helveg, S.; Sehested, J.; Hansen, P. L.; Garzon, F.; Datye, A. K. *J. Am. Chem. Soc.* **2011**, *133*, 20672.
(27) Sá, J.; Taylor, S. F. R.; Daly, H.; Goguet, A.; Tiruvalam, R.; He, Q.; Kiely, C. J.; Hutchings, G. J.; Hardacre, C. *ACS Catalysis* **2012**, *2*, 552.
(28) Li, W. X.; Stampfl, C.; Scheffler, M. *Phys. Rev. Lett.* **2003**, *90*, 256102.
(29) Li, W. X.; Osterlund, L.; Vestergaard, E. K.; Vang, R. T.; Matthiesen, J.; Pedersen, T. M.; Laegsgaard, E.; Hammer, B.; Besenbacher, F. *Phys. Rev. Lett.* **2004**, *93*, 146104.
(30) Feibelman, P. J. *Phys. Rev. Lett.* **2000**, *85*, 606.

(31) Thiel, P. A.; Shen, M.; Liu, D. J.; Evans, J. W. *J. Phys. Chem. C* **2009**, *113*, 5047.
(32) Evans, J. W.; Thiel, P. A. *Science* **2010**, *330*, 599.
(33) Thiel, P. A.; Shen, M.; Liu, D. J.; Evans, J. W. *J. Vac. Sci. Technol. A* **2010**, *28*, 1285.
(34) Tao, F.; Dag, D.; Wang, L. W.; Liu, Z.; Butcher, D. R.; Bluhm, H.; Salmeron, M.; Somorjai, G. A. *Science* **2010**, *327*, 850.
(35) Evans, J.; Hayden, B.; Mosselmans, F.; Murray, A. *Surf. Sci.* **1994**, *301*, 61.
(36) Evans, J.; Hayden, B.; Mosselmans, F.; Murray, A. *Surf. Sci.* **1992**, *279*, L159.
(37) Berkó, A.; Solymosi, F. *J. Catal.* **1999**, *183*, 91.
(38) Frank, M.; Bäumer, M. *Phys. Chem. Chem. Phys.* **2000**, *2*, 3723.
(39) Suzuki, A.; Inada, Y.; Yamaguchi, A.; Chihara, T.; Yuasa, M.; Nomura, M.; Iwasawa, Y. *Angew. Chem., Int. Ed.* **2003**, *42*, 4795.
(40) McClure, S. M.; Lundwall, M. J.; Goodman, D. W. *Proc. Natl. Acad. Sci. U.S.A.* **2011**, *18*, 931.
(41) Rickard, J. M.; Genovese, L.; Moata, A.; Nitsche, S. *J. Catal.* **1990**, *121*, 141.
(42) Lai, X.; Goodman, D. W. *J. Mol. Catal. A: Chem.* **2000**, *162*, 33.
(43) Zhou, J.; Kang, Y. C.; Chen, D. A. *J. Phys. Chem. B* **2003**, *107*, 6664.
(44) Zhou, J.; Kang, Y. C.; Ma, S.; Chen, D. A. *Surf. Sci.* **2004**, *562*, 113.
(45) Datye, A. K.; Xu, Q.; Kharas, K. C.; McCarty, J. M. *Catal. Today* **2006**, *111*, 59.
(46) Simonsen, S. B.; Chorkendorff, I.; Dahl, S.; Skoglundh, M.; Sehested, J.; Helveg, S. *J. Am. Chem. Soc.* **2010**, *132*, 7968.
(47) Simonsen, S. B.; Chorkendorff, I.; Dahl, S.; Skoglundh, M.; Sehested, J.; Helveg, S. *J. Catal.* **2011**, *281*, 147.
(48) Ernst, K. H.; Ludviksson, A.; Zhang, R.; Yoshihara, J.; Campbell, C. T. *Phys. Rev. B* **1993**, *47*, 13782.
(49) Campbell, C. T. *Surf. Sci. Rep.* **1997**, *27*, 1.
(50) Kolmakov, A.; Goodman, D. W. *Catal. Lett.* **2000**, *70*, 93.
(51) Birgersson, H.; Eriksson, L.; Boutonnet, M.; Järås, S. G. *Appl. Catal., B* **2004**, *54*, 193.
(52) Galisteo, F. C.; Mariscal, R.; Granados, M. L.; Fierro, J. L. G.; Daley, R. A.; Anderson, J. A. *Appl. Catal., B* **2005**, *59*, 227.
(53) Romero-Sarria, F.; Martinez, T., L. M.; Centeno, M. A.; Odriozola, J. A. *J. Phys. Chem. C* **2007**, *111*, 14469.
(54) Breen, J. P.; Burch, R.; Hardacre, C.; Hill, C. J.; Krutzsch, B.; Bandl-Konrad, B.; Jobson, E.; Cider, L.; Blakeman, P. G.; Peace, L. J.; Twigg, M. V.; Preis, M.; Gottschling, M. *Appl. Catal., B* **2007**, *70*, 36.
(55) Goguet, A.; Hardacre, C.; Harvey, I.; Narasimharao, K.; Saih, Y.; Sa, J. *J. Am. Chem. Soc.* **2009**, *131*, 6973.
(56) Campbell, C. T.; Parker, S. C.; Starr, D. E. *Science* **2002**, *298*, 811.
(57) Harris, P. J. F. *Nature* **1986**, *323*, 792.
(58) Hansen, P. L.; Wagner, J. B.; Helveg, S.; Rostrup-Nielsen, J. R.; Clausen, B. S.; Topsøe, H. *Science* **2002**, *295*, 2053.
(59) Nolte, P.; Stierle, A.; Jin-Phillipp, N. Y.; Kasper, N.; Schulli, T. U.; Dosch, H. *Science* **2008**, *321*, 1654.
(60) Simonsen, S. B.; Chorkendorff, I.; Dahl, S.; Skoglundh, M.; Meinander, K.; Jensen, T. N.; Lauritsen, J. B.; Helveg, S. *J. Phys. Chem. C* **2012**, *116*, 5646.
(61) Jak, M. J. J.; Konstapel, C.; van Kreuningen, A.; Verhoeven, J.; Frenken, J. W. M. *Surf. Sci.* **2000**, *457*, 295.
(62) Köhn, A.; Weigend, F.; Ahlrichs, R. *Phys. Chem. Chem. Phys.* **2001**, *3*, 711.
(63) Roldán, A.; Viñes, F.; Illas, F.; Ricart, J. M.; Neyman, K. M. *Theor. Chem. Acc.* **2008**, *120*, 565.
(64) Chase, M. W.; Davies, C. A.; Downey, J. R.; Frurip, D. J.; McDonald, R. A.; Syverud, A. N. JANAF Thermochemical Tables, 3rd ed. *J. Phys. Chem. Ref. Data* **1985**, *14*, Suppl. 1.
(65) Reuter, K.; Scheffler, M. *Phys. Rev. B* **2001**, *65*, 035406.
(66) Houk, L. R.; Challa, S. R.; Grayson, B.; Fanson, P.; Datye, A. K. *Langmuir* **2009**, *25*, 11225.
(67) Behafarid, F.; Cuenya, B. R. *Surf. Sci.* **2012**, *60*, 908.
(68) Dadyburjor, D. B.; Marsh, S. P.; Glicksman, M. E. *J. Catal.* **1986**, *99*, 358.
(69) Theis, W.; Bartelt, N. C.; Tromp, R. M. *Phys. Rev. Lett.* **1995**, *75*, 3328.
(70) Bartelt, N. C.; Theis, W.; Tromp, R. M. *Phys. Rev. B* **1996**, *54*, 11741.
(71) Morgenstern, K.; Rosenfeld, G.; Comsa, G. *Surf. Sci.* **1999**, *441*, 289.
(72) Morgenstern, K.; Rosenfeld, G.; Comsa, G.; Sorensen, M. R.; Hammer, B.; Laegsgaard, E.; Besenbacher, F. *Phys. Rev. B* **2001**, *63*, 045412.
(73) Datye, A. K.; Xu, Q.; Kharas, K. C.; McCarty, J. M. *Catal. Today* **2006**, *111*, 59.
(74) Larsson, E. M.; Millet, J.; Gustafsson, S.; Skoglundh, M.; Zhdanov, V. P.; Langhammer, C. *ACS Catalysis* **2012**, *2*, 238.
(75) Reuter, K.; Scheffler, M. *Phys. Rev. B* **2003**, *68*, 045407.
(76) Kresse, G.; Furthmuller, J. *Phys. Rev. B* **1996**, *54*, 11169.
(77) Overbury, S. H.; Bertrand, P. A.; Somorjai, G. A. *Chem. Rev.* **1975**, *75*, 547.
(78) Smedh, M.; Beutler, A.; Borg, M.; Nyholm, R.; Andersen, J. N. *Surf. Sci.* **2001**, *491*, 115.
(79) Zeng, Z. H.; Da Silva, J. L. F.; Li, W. X. *Phys. Chem. Chem. Phys.* **2010**, *12*, 2459.
(80) Chaâbane, N.; Lazzari, R.; Jupille, J.; Renaud, G.; Soares, E. A. *J. Phys. Chem. C.* **2012**, *116*, 23362.